PNAS RESEARCH ARTICLE | BIOPHYSICS AND COMPUTATIONAL BIOLOGY

Topology of molecular deformations induces triphasic catch bonding in selectin–ligand bonds

Casey O. Barkan[a,1] and Robijn F. Bruinsma[a]

Edited by Andrea Liu, University of Pennsylvania, Philadelphia, PA; received September 14, 2023; accepted December 15, 2023

Among the long-standing efforts to elucidate the physical mechanisms of protein–ligand catch bonding, particular attention has been directed at the family of selectin proteins. Selectins exhibit slip, catch–slip, and slip–catch–slip bonding, with minor structural modifications causing major changes in selectins' response to force. How can a single structural mechanism allow interconversion between these various behaviors? We present a unifying theory of selectin–ligand catch bonding, using a structurally motivated free energy landscape to show how the topology of force-induced deformations of the molecular system produces the full range of observed behaviors. We find that the pathway of bond rupture deforms in non-trivial ways, such that unbinding dynamics depend sensitively on force. This implies a severe breakdown of Bell's theory—a paradigmatic theory used widely in catch bond modeling—raising questions about the suitability of Bell's theory in modeling other catch bonds. Our approach can be applied broadly to other protein–ligand systems.

mechanobiology | catch bonding | mechanical allostery | switch point theory

Significance

Selectin–ligand bonds play an essential role in the immune system and have been a central focus of research in mechanobiology. These bonds show several distinct varieties of catch bonding, a counterintuitive phenomenon in which a bond strengthens when stretched by a force. Much theoretical progress has been made in understanding these behaviors, yet prior models cannot explain the full range of observations on selectin–ligand bonds. We present a structural model of selectin–ligand bonds, and we introduce a method that reveals how the various observed behaviors are induced by topologically distinct deformations of the molecular system. This method can be applied to more complex bonds, such as those involving T-cell and B-cell receptors, in future work.

Mechano-sensitive proteins serve a wide range of roles in the immune system, in cell development, and cell migration (1–5). Numerous protein–ligand bonds exhibit catch–slip bonding (6–14), where the bond's strength varies nonmonotonically under an applied pulling force, first strengthening then weakening. Some proteins exhibit even more complex behavior: E-selectin and integrin form slip–catch–slip (triphasic) bonds with certain ligands (8, 15). These counterintuitive responses to force have attracted much interest over the last two decades, with numerous models having been proposed (7, 16–24). Yet, unresolved questions remain regarding the proposed models for the selectin family of proteins [L-, P-, and E-selectin (25)]. The models proposed to explain triphasic bonding either cannot account for the observed bond lifetime distributions, or appear inconsistent with selectin's structure. Hence, it has remained an open question how triphasic bonding is produced in E-selectin, and how its mechanism relates to the mechanisms of slip and catch–slip bonding in P- and L-selectin. The structural features of selectin that mediate ligand binding have similarities to many other mechano-sensitive proteins (23), so investigating this open question holds broader importance for mechanobiology.

The complex nature of mechanobiological systems makes modeling and model validation a challenge. Even the simplest models tend to have many fitting parameters. For example, the simple two-state catch bond model (7, 19) requires eight fitting parameters, and in free energy landscape models one can introduce arbitrarily many fitting parameters. How can one explore, validate, and/or falsify a model while avoiding overfitting? In this work, we present an approach to address this issue. We develop a structural model of selectin–ligand bonds and we introduce a topological approach for classifying the mechanochemistry of the system. This topological approach allows for classification of a model's qualitative behaviors without fine-tuning fitting parameters. With this approach, we show how selectin's structure produces the full range of experimentally observed behaviors: slip, catch–slip, and slip–catch–slip bonding. Our approach builds upon theoretical advances showing that catch bonding can be produced by force-induced deformation of a bond's bound state and transition state (21, 22, 26–33).

At the heart of selectin's distinctive mechanochemistry is an allosteric linkage between the ligand binding site and an interdomain hinge (3, 34). Soon after the experimental discovery of selectin catch–slip bonding, it was recognized that such allostery could generate this behavior (7, 35). However, it was not proposed that this simple mechanism could also generate slip–catch–slip behavior. Our topological approach reveals that even the simplest form of allostery contains the essential physics to produce slip–catch–slip bonding. Furthermore, this allostery provides a sensitive mechanism by which evolution can tune bond behavior. Hence, our model

Author affiliations: [a]Department of Physics and Astronomy, University of California, Los Angeles, CA 90095

Author contributions: C.O.B. and R.F.B. designed research; C.O.B. performed research; and C.O.B. wrote the paper.

The authors declare no competing interest.

This article is a PNAS Direct Submission.

[1]To whom correspondence may be addressed. Email: barkanc@ucla.edu.

This article contains supporting information online at https://www.pnas.org/lookup/suppl/doi:10.1073/pnas.2315866121/-/DCSupplemental.

Published January 31, 2024.

presents a unified theory of selectin catch bonding, accounting for the observed slip, catch–slip, and slip–catch–slip behaviors, as well as the observed distribution of bond lifetimes in each case.

Our finding that force-induced molecular deformations significantly alter unbinding dynamics has important implications for the theory of mechanochemistry. We demonstrate that Bell's theory (36)—a paradigmatic theory invoked by influential catch bond models such as the two-pathway model (17, 18), two-state model (19, 37), and sliding-rebinding model (20)—must break down in selectins. Of course, it is known theoretically that Bell's theory, founded upon the frozen landscape approximation, will break down at large forces. Our model implies that even low forces cause large-scale conformational change to the system's transition state, leading to severe violation of the frozen landscape approximation. This motivates a reexamination of other catch bonds previously modeled using Bell's theory. Furthermore, this brings into question the suitability of steered molecular dynamics (MD) to study protein–ligand unbinding. Though widely used to study catch bonding (20, 38–40), the artificially strong forces used in steered MD may drastically alter the unbinding dynamics.

We begin by modeling the allosteric mechanism that underlies selectin's mechanochemistry (Section I), then we show how the model's behaviors can be classified based on the topology of molecular deformations (Section II). We show quantitative comparison between our model and experimental data (Section III), then discuss the inadequacy of Bell's theory in explaining selectins' behaviors, and discuss how our model builds upon prior work (Section IV).

I. Modeling the Allosteric Mechanism

Selectin proteins have been heavily studied due to their importance in initiating inflammatory response (3, 25, 41). As a result, extensive data is available which we use to construct and test our model. Selectin comes in three varieties: *P-selectin* (the first experimentally verified catch bond (6)), *L-selectin*, and *E-selectin* (which is the only selectin found to exhibit slip–catch–slip behavior (15)). Selectins extend into the bloodstream from the membranes of epithelial cells, leukocytes, and platelets, where they bind ligands (chiefly PSGL-1) expressed on the surface of leukocytes traveling in the bloodstream (25). The tip of a selectin protein, where ligand binding occurs, is comprised of a lectin and an EGF-like domain connected by an interdomain hinge. Fig. 1*A* shows the structure of these domains (teal) bound to the ligand PSGL-1 (magenta) (42).

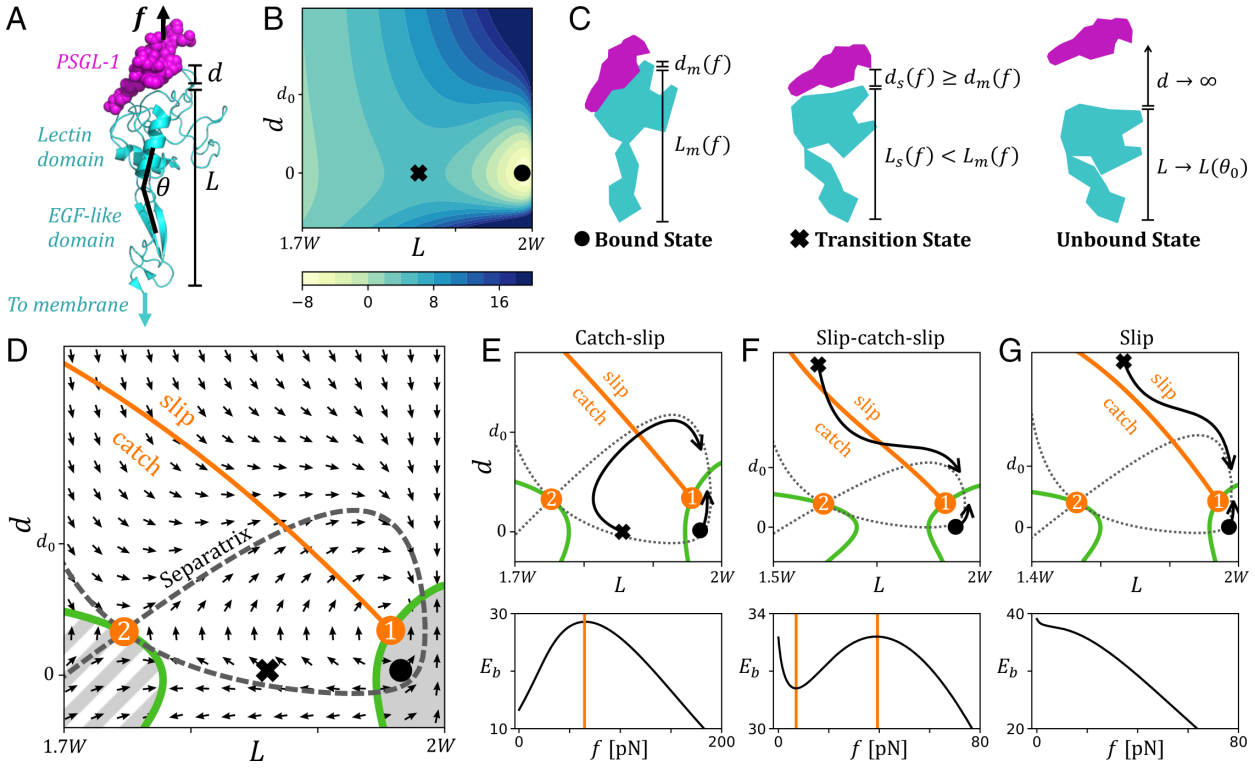

Fig. 1. Force-induced deformation of selectin–ligand bonds. (*A*) Structure of P-selectin bound to PSGL-1 (PDB ID code: 1G1S (42), rendered in PyMOL), with interdomain hinge angle θ, protein extension L, and distance d between the binding site and ligand. (*B*) Free energy landscape $V_f(L, d)$ at $f = 0$ (with parameters for L-selectin–PSGL-1 listed in Table 1). The color bar indicates values of V_f in units of k_BT, where 0 is the free energy of the unbound ($d \to \infty$) state. The minimum point (i.e. bound state ●) and saddle point (i.e. transition state ✖) are indicated. Note that $d = 0$ corresponds to the lowest-energy bond length at zero force (hence, $d < 0$ indicates bond lengths less than this length). (*C*) Cartoon structures of selectin (teal) and ligand (magenta) in the bound state $\boldsymbol{x}_m(f) = (L_m(f), d_m(f))$, transition state $\boldsymbol{x}_s(f) = (L_s(f), d_s(f))$, and unbound state. (*D*) Flow of bound state and transition state under increasing f. The $\det(H)=0$ curves (green), switch points (orange dots), and separatrix (dashed gray curve) are shown. The solid gray shaded region is the minimum-like region containing the bound state. The striped gray region is the minimum-like region with no local minimum. The white region is the saddle-like region containing the transition state. The orange curve indicates the switch line, separating the "catch" region from the "slip" region. ● and ✖ indicate the bound state and transition state for one choice of model parameters (given in *SI Appendix*, section 1). (*E–G*) Upper plots: trajectories $\boldsymbol{x}_m(f)$ and $\boldsymbol{x}_s(f)$ (solid black curves), switch points (orange dots), switch line (orange curve), $\det(H)=0$ curves (green), and separatrix (dashed gray). Each panel uses a different choice of model parameters, generating different initial conditions $\boldsymbol{x}_m(0)$ and $\boldsymbol{x}_s(0)$, which lead to different bond behavior (catch–slip, slip–catch–slip, or slip). Lower plots: The corresponding energy barrier $E_b(f)$ in pNnm. The orange bar indicates the switch between increasing and decreasing E_b, corresponding to the point where $\boldsymbol{x}_s(f)$ crosses the switch line.

An allosteric linkage between the binding site and the interdomain hinge was revealed by experiments on mutated forms of selectin (34, 43). These studies found that selectins bind PSGL-1 most tightly when the interdomain hinge is in an extended conformation (large θ, as indicated in Fig. 1*A*), and binding weakens as θ decreases. Analysis of X-ray crystallography structures of P-selectin in both a bent and extended configuration (achieved by crystallizing P-selectin both with and without a bound ligand (42)) revealed that the hinge angle affects the arrangement of amino acid side chains at the binding interface that form hydrogen bonds with the ligand; for large θ, additional hydrogen bonds are able to form, strengthening binding (23, 34). However, the X-ray structures also imply that the hinge energetically prefers a bent angle (smaller θ), which opposes strong ligand binding.

The interplay between the hinge's energetic preference for small θ, and the binding site's preference for large θ when a ligand is bound, produces catch–slip bonding for the following reason: a pulling force on the ligand causes θ to increase, strengthening the bond (i.e. catch behavior, defined by increasing mean bond lifetime under increasing force). As the hinge approaches its full extension, increasing force can no longer increase θ, so the bond switches to slip behavior (defined by decreasing mean lifetime under increasing force). Hence, this simple allosteric mechanism can explain catch–slip behavior. However, can it explain slip–catch–slip behavior? We use a minimal model to investigate this question.

A minimal model for the free energy of the selectin–ligand system should retain only the essential degrees of freedom—those that are both slow and contribute nonharmonically to the free energy (harmonic contributions can be course-grained out, see *SI Appendix*, section 2). The allosteric coupling between the hinge and binding site implies a nonharmonic coupling between θ and the distance d between binding site and ligand, so a minimal free energy landscape should depend on θ and d. However, rather than express the free energy explicitly in terms of θ, it is convenient to instead use the θ-dependent extension of the protein, L, as indicated in Fig. 1*A*. L is related to θ by $L(\theta) = 2W\sin(\theta/2)$ and inversely, $\theta(L) = 2\arcsin(L/2W)$, where W is the length of the lectin and EGF-like domains (the two domains are nearly the same length, and we estimate $W \approx 2.8$ nm). Our model free energy is the following modified form of the model introduced in ref. 33:

$$V_f(L,d) = V_\theta(\theta(L)) + B(d,\theta(L)) - (L+d)f. \qquad [1]$$

The term $V_\theta(\theta) = \frac{1}{2}k_\theta(\theta-\theta_0)^2$ describes the hinge's energetic preference for a bent conformation (3, 34) with preferred angle θ_0 (we estimate $\theta_0 \approx 0.58\pi$ from the published structure). Binding to the ligand is described by a Morse potential $B(d,\theta) = D(\theta)[(1-e^{-d/d_0})^2 - 1]$, where the angle-dependent binding strength $D(\theta)$ captures the allostery between the hinge and binding site. The true form of $D(\theta)$ is presumably complicated and tuned through evolution to serve selectins' functions. Nevertheless, a simple form for $D(\theta)$ should capture the essential physics of the system. A minimal form uses a Gaussian peaked at an extended angle θ_1: $D(\theta) = D_0\exp[-(\theta-\theta_1)^2/2\sigma^2]+c$. This minimal form is sufficient to qualitatively explain all observed behaviors of selectins. The final term in Eq. **1**, which describes the system's coupling to the pulling force, is determined by the work done by the pulling force in bringing the system to configuration (L,d). Note that we do not define the coordinates L and d at the level of individual atoms, because such a specification cannot be validated using a coarse-grained model. Future work involving MD simulations may allow atomic-level definitions of these collective variables (*Discussion*).

Fig. 1*B* shows the free energy landscape for $f = 0$ using the best-fit parameters for the L-selectin–PSGL1 bond (as described in Section III). The local minimum (●), corresponding to the bound state, and saddle point (✖), corresponding to the transition state, are indicated. *SI Appendix*, Fig. S1*A* shows how the free energy landscape changes as f increases. Fig. 1*C* shows cartoons of the structures of the bound state, transition state, and unbound state. Importantly, these structures are force-dependent, and their force-induced deformations are key to our analysis in Section II.

To compare the model to experimental data, predicted mean bond lifetimes τ must be estimated from the model. Approximate mean bond lifetime predictions can be obtained from the Arrhenius law,

$$\tau \approx \tau_0\exp[(V_f(\boldsymbol{x}_s) - V_f(\boldsymbol{x}_m))/k_BT], \qquad [2]$$

where the vectors $\boldsymbol{x}_m = (L_m, d_m)$ and $\boldsymbol{x}_s = (L_s, d_s)$ denote, respectively, the positions in configuration space of the local minimum (the bound state) and saddle point (the transition state) of V_f. The structural meaning of these quantities is illustrated in Fig. 1*C*. For large energy barrier $E_b \equiv V_f(\boldsymbol{x}_s) - V_f(\boldsymbol{x}_m)$, Eq. **2** provides a good approximation and the prefactor τ_0 can be approximated using Langer's formula (44). However, to ensure accuracy, we compute τ by numerically solving the Fokker–Planck equation (*Materials and Methods*).

Importantly, experiments measure not only mean lifetime, but also lifetime distribution, and models that correctly predict mean lifetime may not correctly predict the distribution of lifetimes. For a system with a single bound state, the lifetime distribution is approximately exponential: for mean lifetime τ, the probability distribution for bond lifetime is $p_\tau(t) = \frac{1}{\tau}e^{-t/\tau}$ (*SI Appendix*, section 3). However, in a system with multiple bound states, the lifetime distribution is multi-exponential; for example, FimH-mannose has two bound states and a double-exponential lifetime distribution (7). All lifetime distribution data for selectins show a single-exponential decay (6, 15, 45), indicating only one bound state. Our proposed free energy is consistent with this experimental data, as shown by the single local minimum in Fig. 1*B*.

II. Topology of Molecular Deformations

Eq. **2** illustrates why force-induced deformation of the bound state $\boldsymbol{x}_m$ and transition state $\boldsymbol{x}_s$ are key to a system's mechanochemistry. Under increasing f, these deformations are described by trajectories $\boldsymbol{x}_m(f)$ and $\boldsymbol{x}_s(f)$ through the system's configuration space, generating force-dependent bond lifetime $\tau(f)$. Topological classification of these trajectories enables qualitative predictions of a bond's behavior without any parameter fitting.

Writing the free energy in the general form $V_f(\boldsymbol{x}) = V(\boldsymbol{x}) - f\boldsymbol{\ell}\cdot\boldsymbol{x}$ (for Eq. **1**, $\boldsymbol{x} = (L,d)$ and $\boldsymbol{\ell} = (1,1)$), the trajectories $\boldsymbol{x}_m(f)$ and $\boldsymbol{x}_s(f)$ obey (29, 32, 33)

$$\frac{d}{df}\boldsymbol{x}_i = H^{-1}(\boldsymbol{x}_i)\boldsymbol{\ell}, \qquad [3]$$

where $i = m$ or s and where $H(\boldsymbol{x})$ is the Hessian matrix of $V(\boldsymbol{x})$. A system's catch bonding behavior is generated by the flow defined by this equation. Specifically, it was recently shown that force-induced switching between catch and slip behavior is generated

by singularities in the flow, called switch points (33) (specifically, ℓ-switch points, to distinguish them from $\boldsymbol{n}$-switch points; see *Materials and Methods*). The flow for our selectin model is shown by the vector field in Fig. 1*D*. ℓ-switch points are shown as orange dots labeled 1 and 2. Switch points lie along the boundaries between regions where $V(\boldsymbol{x})$ has "minimum-like" curvature (where $\det(H)>0$, shaded gray or striped in Fig. 1*D*) and regions with "saddle-like" curvature (where $\det(H)<0$, shaded white). These boundaries, where $\det(H)=0$, are shown by green curves. A simple geometric criterion determines the location of switch points on the $\det(H)=0$ curves (*Materials and Methods*). In Fig. 1*D*, the minimum-like region shaded solid gray contains the bound state, whereas the minimum-like region shaded striped gray contains either no local minimum or an extremely shallow local minimum (less than $0.3k_BT$ and existing only for $f < 2$ pN) in the range of parameters relevant for selectin.

ℓ-switch points shape the flow in the same way that a dynamical system's fixed points shape its phase portrait. In fact, ℓ-switch points are fixed points of the regularized flow defined in *Materials and Methods*. Switch point 1 induces circulating (locally elliptic) trajectories and switch point 2 induces locally hyperbolic trajectories. A separatrix extends from switch point 2 along the asymptotes of the hyperbolic flow (dashed gray curve in Fig. 1*D*). The separatrix separates topologically distinct families of trajectories. Trajectories enclosed within the separatrix can produce catch–slip behavior, while trajectories above the separatrix can produce slip–catch–slip behavior, as we explain below.

The initial conditions of Eq. **3**, i.e., the bound state and transition state at zero force $\boldsymbol{x}_m(0)$ and $\boldsymbol{x}_s(0)$, depend on the model parameters. $\boldsymbol{x}_m(0)$ and $\boldsymbol{x}_s(0)$ for one choice of parameters are indicated by (●) and (✖) in Fig. 1*D*. If the parameters are changed, the initial conditions will change, as in Fig. 1 *E*–*G*. Importantly, the topology of the flow and of the $\det(H)=0$ curve are invariant under changes in the model parameters (though very large parameter changes can modify the topology, see *SI Appendix*, section 1 and Fig. S3*B*). Fig. 1 *E*–*G* illustrate how the $\det(H)=0$ curve and separatrix change shape under changes in parameters, but, topologically, they remain the same.

The trajectories $\boldsymbol{x}_m(f)$ and $\boldsymbol{x}_s(f)$ shown in Fig. 1 *E*–*G*, illustrate how the model can exhibit catch–slip, slip–catch–slip, and slip behaviors—exactly those behaviors observed in experiments on selectins. These figures show the switch line (orange curve) that extends from switch point 2. The switch line indicates where the energy barrier $E_b(f)$ switches from increasing to decreasing under increasing force f (calculation of the path of the switch line is described in *Materials and Methods*). The energy barrier is increasing (catch behavior) when $\boldsymbol{x}_s$ is to the bottom-left of the switch line, and the energy barrier is decreasing (slip behavior) when $\boldsymbol{x}_s$ is to the top-right. Catch–slip bonding is produced by trajectories enclosed within the separatrix that cross the switch line once (Fig. 1*E*), and slip–catch–slip behavior is produced by trajectories above the separatrix that cross the switch line twice (Fig. 1*F*). For some initial conditions, the trajectory does not cross the switch line at all (Fig. 1*G*), producing only slip behavior. Hence, from a minimal structural model, we can qualitatively explain the full range of observed behaviors while avoiding parameter fine-tuning.

III. Quantitative Comparison to Data

While the previous section shows that the model can qualitatively capture the observed behaviors of selectin–ligand bonds, it is illuminating to quantitatively fit the model to data. Quantitative fits give insight into how trends in the experimental data relate to structural differences between different forms of selectin. Furthermore, the fits reveal how the allosteric linkage $D(\theta)$ can tune the response to force, illustrating how a wide range of behaviors may have evolved from the same simple mechanism. However, overfitting is a concern. Reassuringly, the best-fit parameters for our model are physically reasonable and the fits are obtained with between 4 and 6 free parameters (on par with or better than prior catch bond models); the method for obtaining best-fit parameters is described in *SI Appendix*, section 1. Nevertheless, as with all published catch bond models, the best-fit parameters should be interpreted judiciously.

Table 1. Best-fit model parameters

Selectin	Ligand	k_θ	D_0	d_0	σ/π	θ_1/π	c
L-selectin	PSGL1	266	237	0.29	0.12	1 (*)	0 (*)
LSelN138G	PSGL1	220	210	0.29	0.12	1 (*)	0 (*)
L-selectin	2GSP6	266	217	0.33	0.09	0.98	0 (*)
LSelA108H	2GSP6	266	201	0.33	0.17	0.97	0 (*)
P-selectin	sPSGL1	167	240	0.59	0.10	0.90	0 (*)
E-selectin	sLe^x	273	207	0.26	0.18	1.0	9.5

Units: k_θ (pNnm), D_0 (pNnm), d_0 (nm), σ (radians), θ_1 (radians), c (pNnm). (*) indicates parameters that were fixed at preset values during fitting. For all selectin–ligand pairs, W=2.8 nm and $\theta_0 = 0.58\pi$ were assumed, as estimated from structure.

Fig. 2*A* shows the best-fit bond lifetime predictions for L-selectin bound to PSGL-1 (black curve), which agrees closely with experimental data (black diamonds, (46)). The best-fit parameters are given in Table 1. Fig. 2*B* shows the trajectories $\boldsymbol{x}_m(f)$ and $\boldsymbol{x}_s(f)$ generated using the best-fit parameters. As expected for catch–slip behavior, the trajectories are enclosed within the separatrix, so $\boldsymbol{x}_s(f)$ crosses the switch line once. Computing predicted lifetimes requires an estimate of the friction coefficient γ. As discussed in *Materials and Methods*, Stokes' law sets a lower bound of $\gamma \gtrsim 10^{-7}$ pN s/nm, and experiments on high-friction proteins suggest an upper bound of $\gamma \lesssim 10^{-2}$ pN s/nm (48). From parameter fitting, we estimate $\gamma \approx 3\times10^{-5}$ pN s/nm, roughly halfway between these bounds.

A key feature of the allosteric mechanism is that the "spring" of the hinge (described by k_θ) energetically opposes ligand binding (described by D_0) because binding is strongest when the hinge is extended away from its lowest-energy bent angle. This feature is reflected in the best-fit parameters: even though k_θ and D_0 are both very large (62 k_BT and 55 k_BT, respectively), the energy barrier for bond rupture is much smaller (12 k_BT at $f = 0$ and 16 k_BT at $f = 64$ pN) because the transition state finds a balance between these opposing forces.

A mutated form of L-selectin, LSelN138G, in which a key amino acid at the interdomain hinge is mutated, was found to shift the catch–slip switch to lower force and to moderately increase the maximum lifetime (Fig. 2*A* orange squares, (46)). This mutation at the interdomain hinge could be expected to modify the hinge spring constant k_θ and the strength of the allosteric linkage. Indeed, the close agreement between model prediction and data for LSelN138G (Fig. 2*A*, orange) was obtained by modifying only k_θ and D_0 relative to the L-selectin–PSGL-1 best-fit parameters. A different mutation, within the binding site of L-selectin, converts L-selectin's catch behavior into slip behavior when bound to the ligand 2-GSP-6 (47). Fig. 2*C* shows data for L-selectin (black diamonds) and the mutated form LSelA108H (orange squares). Because this mutation is located in the binding site, we expect the hinge parameters to be unaffected by this change. Indeed, only the parameters D_0,

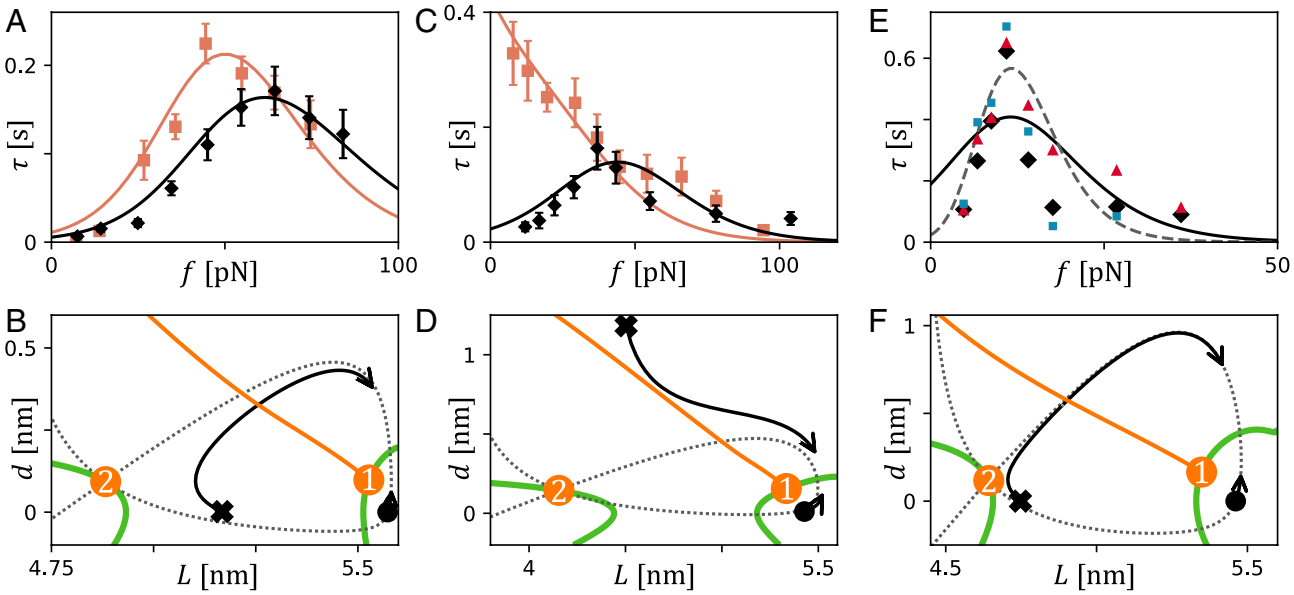

Fig. 2. Comparison of theory and data for L- and P-selectin. (*A*) L-selectin (black) and LSelN138G (orange) bound to PSGL-1. Model predictions (solid curves) and mean bond lifetime (data squares/diamonds, (46)). Best fit parameters given in Table 1. (*B*) Trajectories $\boldsymbol{x}_s(f)$ and $\boldsymbol{x}_m(f)$ for L-selectin–PSGL-1. (*C*) L-selectin (black) and LSelA108H (orange) bound to 2-GSP-6. Model predictions (solid curves) and mean bond lifetime data (squares/diamonds, (47)). This single amino acid mutation converts the catch–slip bond to a slip bond. (*D*) Trajectories $\boldsymbol{x}_s(f)$ and $\boldsymbol{x}_m(f)$ for LSelA108H–2-GSP-6. (*E*) P-selectin bound to sPSGL-1. Model prediction (solid black curve), model with increased lever arm $W_{\text{eff}} = 15$nm (dashed grey curve, see *SI Appendix*, section 1), and data of mean bond lifetime (black diamonds), SD of bond lifetimes (red triangles), and -1/slope of lifetime distribution (blue squares) (6). (*F*) Trajectories $\boldsymbol{x}_s(f)$ and $\boldsymbol{x}_m(f)$ for P-selectin–sPSGL-1. In panels *B*, *D*, and *F*, the switch points and switch line (orange), det H=0 curve (green) and separatrix (dashed gray) are shown.

σ, and θ_1 are modified to convert the model from L-selectin's catch–slip behavior to LSelA108H's slip behavior. As expected, the trajectories $\boldsymbol{x}_s(f)$ and $\boldsymbol{x}_m(f)$ for this bond (Fig. 2*D*) are topologically equivalent to those in Fig. 2*G*, where $\boldsymbol{x}_s(f)$ does not cross the switch line.

P-selectin shows a sharper catch–slip response than L-selectin, occurring over a narrower range of forces and reaching a larger maximum lifetime. Fig. 2*E* shows experimental bond lifetime data for P-selectin–sPSGL-1 (6). The data points show average measured lifetime (black squares), SD of measured lifetimes (red triangles), and negative inverse slopes of measured lifetime distributions (blue squares). The spread in these three quantities roughly indicates the uncertainty in mean lifetime because, for an idealized bond, the three quantities would be equal (6). A qualitative, but not quantitative, fit to experimental data is obtained (Fig. 2*E* black curve, parameters in Table 1). A possible reason for the discrepancy is that the lever arm with which the force acts on the hinge θ may be longer than W due to both the ligand and consensus repeat domains of selectin. Assuming a larger lever arm substantially improves the fit (Fig. 2*E* dashed grey cruve); see *SI Appendix*, section 1 for details. The trajectories $\boldsymbol{x}_s(f)$ and $\boldsymbol{x}_m(f)$ are, as expected, enclosed within the separatrix with $\boldsymbol{x}_s(f)$ crossing the switch line once (Fig. 2*F*).

The slip–catch–slip behavior of E-selectin can be qualitatively described by the model in its minimal form (i.e. using the Gaussian form for $D(\theta)$), as shown in Fig. 2*A* (data from ref. 15). The trajectories $\boldsymbol{x}_m(f)$ and $\boldsymbol{x}_s(f)$ cross the switch line twice, producing slip–catch–slip behavior (Fig. 2*B*). However, the minimal model fails to capture the narrow peak at the catch–slip switch exhibited in the data. There are many possible explanations for this discrepancy; for example, the true allosteric linkage is certainly more complicated than a simple Gaussian function, and perhaps the narrow peak results from a more intricate linkage. Alternatively, perhaps the simple quadratic form that we assume for $V_\theta(\theta)$ is insufficient. Moreover, perhaps there are additional slow nonharmonic degrees of freedom that must be accounted for in the free energy.

Although we cannot conclude definitively what causes the discrepancy between the minimal model and data for E-selectin, we can investigate whether the data can be explained by a more intricate allosteric mechanism. Specifically, we explore whether a more complex, non-Gaussian, form of $D(\theta)$ can produce a closer fit to data. By augmenting $D(\theta)$ with two lower-amplitude Gaussian functions, we obtain a close fit to the narrow peak in the experimental data (Fig. 2 *C*, *Inset* shows augmented $D(\theta)$). The allosteric linkage in selectin proteins is presumably tuned through evolution to serve selectins' functions, and the effect of augmenting $D(\theta)$ illustrates how the allosteric mechanism allows for evolutionary "tuning" of bond behavior.

IV. Bell's Theory and Prior Models of Selectin–Ligand Bonds

Numerous models of catch bonding have been proposed in the literature, most of which involve a fixed set of bound states connected by force-dependent transition rates given by Bell's theory (36). Such "state-based" models are defined by a set of states (both bound and ruptured states) and pathways between states, with the transition rate from state i to j via pathway p given by $k_{i\to p\to j}(f) = k^o_{i\to p\to j}\exp[f\Delta x_{ip}/k_BT]$. If the rates are constrained to obey detailed balance, then such a model can be viewed as a low-force approximation to a free energy landscape model, where each bound state corresponds to a local minimum of the free energy. This is known as the frozen landscape approximation because it neglects the movement of minimum and saddle points under the flow described by Eq. **3**. In essence, the minimum and saddle points are assumed to be "frozen" in place.

Our finding that $\boldsymbol{x}_s(f)$ and $\boldsymbol{x}_m(f)$ follow the nontrivial trajectories shown in Figs. 2 and 3 illustrates a failure of the

frozen landscape approximation, and, therefore, a breakdown of Bell's theory, for our model of selectin. However, other models have been proposed for selectin that are "state-based," invoking Bell's theory to specify the force-dependent transition rates between states. There are two proposed state-based models of selectin capable of exhibiting slip, catch–slip, and slip–catch–slip behaviors: the two-state model (19, 37) and the sliding-rebinding model (15, 20). These models involve multiple bound states and multiple pathways to the ruptured state; in contrast, our model has just one bound state and one pathway (i.e. one transition state) which continuously deform under force. Can these alternative models explain the data for selectins?

Interestingly, both of these alternative models fail to explain the observed bond lifetime distributions. Fig. 3*D* shows experimental lifetime distribution data for E-selectin (blue diamonds, (15)), as well as our model's prediction (black line) and the two-state model's prediction (orange curve). For the two-state model, the two bound states give rise to a double-exponential lifetime distribution, which is inconsistent with the data. The sliding-rebinding model, which has more than two bound states, suffers the same problem. Further discussion of these two models is given in *SI Appendix*, section 4.

This raises the question: could there be any state-based model invoking Bell's theory that is consistent with experiments on selectins? We prove mathematically that the answer is no. The proof is as follows: the single-exponential form of E-selectin's bond lifetime distributions implies a single bound state. In principle, there could be many pathways from this bound state to the ruptured state(s). If there are N rupture pathways, a state-based model employing Bell's theory would have a rupture rate of:

$$k(f) = \sum_{i=1}^{N} k_i^o e^{\beta f \Delta x_i}, \qquad [4]$$

where $\beta = 1/k_B T$. The constants k_i^o must be positive, while the constants Δx_i may be positive or negative. Note that for $N = 2$ this is the "two-pathway model" (17, 18), which was among the first theories of catch–slip bonding.

For a slip–catch–slip bond, $\frac{d^2}{df^2}k(f)$ is negative at the switch from slip to catch. Yet, taking the second derivative of Eq. **4** yields:

$$\frac{d^2}{df^2}k(f) = \sum_{i=1}^{N} k_i^o (\beta \Delta x_i)^2 e^{\beta f \Delta x_i}, \qquad [5]$$

which is always positive. Therefore, such an N-pathway model cannot generate slip–catch–slip behavior and therefore cannot explain the data for E-selectin. This proves that Bell's theory must break down in selectin–ligand bonds.

More recently, a free energy landscape model of selectin was proposed by Chakrabarti et al. (23) (referred to here as the CHT model), marking a major advance toward a microscopic theory of selectin's catch bonding. This model took a mathematically elegant approach of proposing a free energy landscape for which an exact expression for mean bond lifetime was obtainable through a mean first passage time calculation. The model accurately predicts selectin's catch–slip bond lifetime data, though the model does not exhibit slip–catch–slip behavior. The model also correctly predicts a single-exponential bond lifetime distribution, unlike the prior state-based models. While the special form of the CHT free energy was fruitful in that it allows analytical results, it also raises questions about the accuracy of the model and precludes it from exhibiting slip–catch–slip behavior. First, the model predicts that the transition state occurs at $\theta = 0$ (corresponding to $\theta = \pi$ in the coordinates used in ref. 23) in the catch regime, which would imply a nonphysical overlap of the EGF-like and lectin domains. Second, the free energy landscape involves a "cusp" transition state, where the bond breaks when a coordinate

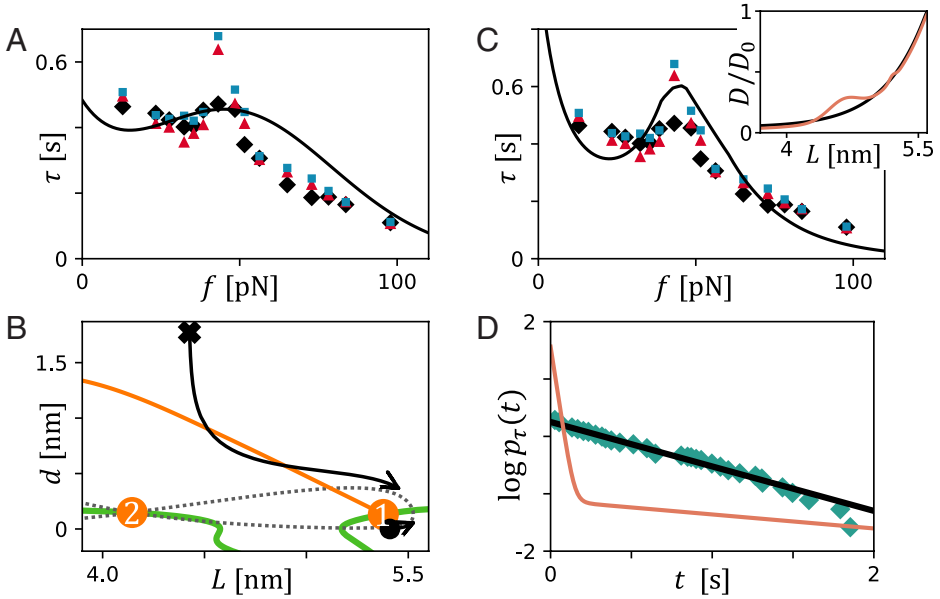

Fig. 3. Slip–catch–slip behavior of E-selectin. (*A*) Qualitative fit to data with the minimal (Gaussian) form of $D(\theta)$. Parameters given in Table 1. Data: mean bond lifetime (black diamonds), SD of bond lifetimes (red triangles), and −1/slope of lifetime distribution (blue squares) (15). (*B*) Trajectories $\boldsymbol{x}_S(f)$ and $\boldsymbol{x}_M(f)$ corresponding to the model prediction in panel *A*. $\boldsymbol{x}_S(f)$ crosses the switch line (orange) twice, indicating the slip-to-catch and catch-to-slip switches. (*C*) Close agreement between theory and data achieved for the augmented allosteric linkage $D(\theta)$. *Inset*: augmented (orange) and Gaussian (black) forms of $D(\theta(L))$. The trajectories $\boldsymbol{x}_S(f)$ and $\boldsymbol{x}_M(f)$ are similar to those in panel *B* except that a second saddle point appears for forces above 68 pN (*SI Appendix*, section 1 and Fig. S3*D*). (*D*) Lifetime distribution for E-selectin at $f = 48$ pN. Data blue squares (15) and our model (black line) show a single-exponential form. However, the two-state model (red) predicts a double-exponential form, inconsistent with the data. Two-state model parameters are given in *SI Appendix*, section 4.

(r, in the coordinates in ref. 23) reaches a critical value. Modeling a free energy function with a cusp is a widely used approximation; however, the cusp removes the large d behavior of the free energy, which, for selectin, "deletes" the portion of the free energy landscape responsible for slip–catch–slip behavior (this is apparent from the trajectory $\boldsymbol{x}_s(f)$ in Fig. 3*B*). In general, a cusp acts to artificially "pin" the location of the saddle point (i.e. $\boldsymbol{x}_s(f)$ is pinned at one position for a range of f), which introduces artifacts.

Our model builds on the pioneering work of the CHT model by using a free energy function that better captures the structural details. As a result, our model captures the full range of experimentally observed behaviors of selectin–ligand bonds.

V. Discussion

We propose a free energy landscape model of selectin–ligand catch bonding which exhibits the full range of experimentally observed bond lifetime behaviors of L-, P-, and E-selectin. By studying the topology of force-induced molecular deformations, we show how a single physical mechanism—an allosteric linkage between interdomain hinge and binding site—produces slip, catch–slip, and slip–catch–slip bonding. This topological approach allows investigation of the qualitative behaviors of the model without any parameter fitting, giving confidence that our results do not rely on finely tuned parameters. Quantitative fits to data are also achieved with physically reasonable fitting parameters, and our model agrees with data of both mean bond lifetime and lifetime distribution. Our finding that bond behavior can be "tuned" by minor changes to the allosteric linkage suggests that selectins employ a highly evolvable mechanism, letting them adapt to a variety evolutionary selection pressures.

Future work applying the theory of switch points to more complex protein systems is forthcoming. T-cell receptor (TCR) binding to pMHC is one exciting system where catch bonding has been observed. Intriguingly, force-induced deformations of TCRs have been suggested to play a key role in T-cell activation (39, 40, 49). However, such a model would necessitate moving beyond the two-dimensional framework used in this work. Fortunately, the theory of switch points can be generalized to higher dimensions (33).

The violation of the frozen landscape approximation exhibited by our model, even at low forces, raises questions about the suitability of Bell's theory for other catch bonds and other complex mechanobiological systems. Future work that develops free energy landscape models of other important catch bonds, such as integrin–fibronectin and FimH–mannose bonds, will clarify whether the frozen landscape approximation is suitable in these systems. FimH is similar to selectin in that it terminates in a lectin domain and involves an allosteric linkage at an interdomain hinge (7, 50). Therefore, a similar model to Eq. **1** may be applicable to FimH. Importantly, FimH–mannose experiments find a double exponential lifetime distribution, necessitating a free energy model with two local minima. In fact, Eq. **1** can have two local minima (one in each minimum-like region) for certain parameter values, consistent with this data. Additionally, it has been suggested that integrin catch–slip and slip–catch–slip bonding is generated by an allosteric hinge mechanism similar to that of selectin (23). Lifetime distributions for the integrin–fibronectin slip–catch–slip bond appear to be triple-exponential (supplement of ref. 8), suggesting a more complex mechanism is at play.

It is possible that experiments could test our predictions by probing force-induced deformations in selectin–ligand bonds or other catch bonds, using atomic force microscopy, optical tweezers, or FRET. Our model of selectin predicts very large deformation of the transition state, yet quite small deformation of the bound state. This presents a difficulty for experiments: molecular systems pass through their transition states extremely rapidly, on far shorter timescales than the temporal resolution of experiments. The deformation of the bound state could plausibly be measured, but the predicted deformations are near or below the spatial resolution of current capabilities (51–53). Other protein–ligand systems with softer bound states that undergo larger deformation may be more suited to such experiments.

An alternative to direct experimental measurement is molecular dynamics (MD) simulations. MD simulation of protein–ligand unbinding is a notoriously difficult problem (54), as typical bond lifetimes (often $\sim$1 s) are vastly longer than feasible simulation times (typically $\lesssim$1 ms). To overcome this issue, steered MD simulations, in which artificially high forces are used to increase unbinding rates, have been employed to study catch bonds (20, 38–40). However, our results show that the transition state of catch bonds can be very sensitive to force; indeed, catch behavior is generated by this sensitivity. Hence, unbinding dynamics observed in steered MD may be drastically different from the dynamics under physiological forces.

A recent work presents an exciting alternative to steered MD, using metadynamics to achieve the first-ever all-atom simulation of protein–ligand slip bonding under physiological forces (54). Future refinements of this technique will likely allow all-atom simulations of catch bonding. This method requires predefined collective variables, and low dimensional models like our selectin model may prove very useful in substantiating choices of collective variables. More generally, low dimensional models and MD simulations should not be viewed as alternatives, but rather as complementary approaches which will likely need to be developed in tandem to provide deeper insights into molecular mechanisms of unbinding.

Materials and Methods

Computing Mean Bond Lifetime from the Fokker–Planck Equation. For a system with potential of mean force (i.e. free energy landscape) $V(\boldsymbol{x})$ and uniform isotropic friction coefficient γ, the Fokker–Planck equation is:

$$\frac{\partial}{\partial t}p(\boldsymbol{x},t) = \frac{1}{\gamma}\nabla\cdot\left(p(\boldsymbol{x},t)\nabla V + I\nabla p(\boldsymbol{x},t)\right). \qquad [6]$$

We assume such uniform isotropic friction to avoid introducing additional fitting parameters. A lower bound for γ can be estimated from Stokes' law $\gamma = 6\pi\eta R$ (55) for a sphere of radius R in a fluid with dynamic viscosity η, which neglects the protein's internal friction. For a protein in water with characteristic size of $R \approx$ 5nm, Stokes' law implies $\gamma \gtrsim 10^{-7}$ pN s/nm. A recent study on a high-friction protein system suggests $\gamma \lesssim 10^{-2}$ pN s/nm (48). We estimate $\gamma \approx 3\times10^{-5}$ pN s/nm for selectin based on fitting model prediction to data.

Mean bond lifetime can be computed from Eq. **6** by computing the quasi-stationary probability current exiting the meta-stable well. By discretizing space, this computation can be reduced to an eigenvector problem that can be numerically solved using standard linear algebra computer packages. We discuss the detailed implementation in *SI Appendix*, section 5.

ℓ- and n-Switch Points, and the Regularized Flow Equation. It was recently shown that the flow (Eq. **3**) has singularities, called ℓ- and n-switch points, that generate force-induced switching behaviors (33). ℓ-switch points generate a switch between catch and slip via a single pathway. ℓ-switch points are located at points on the $\det(H)=0$ curve where $\boldsymbol{v}_0\cdot\boldsymbol{\ell} = 0$, where $\boldsymbol{v}_0$ is the eigenvector

of H with vanishing eigenvalue and where $\boldsymbol{\ell}$ is the force coupling (defined above Eq. **3**). ***n***-switch points indicate a switch in the pathway and are not relevant to the model here.

$\boldsymbol{\ell}$-switch points are similar to the fixed points of a dynamical system. In fact, they are fixed points of the regularized flow equation obtained by the change of variables $du = \det(H)df$:

$$\frac{d}{du}\boldsymbol{x}_i(u) = \text{Adjugate}[H(\boldsymbol{x}_i)]\boldsymbol{\ell}, \qquad [7]$$

where $\text{Adjugate}\left[\begin{smallmatrix} a & b \\ c & d \end{smallmatrix}\right] = \left[\begin{smallmatrix} d & -b \\ -c & a \end{smallmatrix}\right]$ for a 2×2 matrix (in general, $\text{Adjugate}[H] = \det(H)H^{-1}$ at points where $\det(H)\neq 0$). This regularization removes the divergence of Eq. **3** along the $\det(H)=0$ curve (this technique was first used in ref. 56). *SI Appendix*, Fig. S3*C* shows the phase portrait of the regularized flow for our selectin model.

Switch Lines. Switch lines indicate where the energy barrier $E_b(f)$ switches between increasing ($\frac{d}{df}E_b > 0$) and decreasing ($\frac{d}{df}E_b < 0$). Switch lines partition the saddle-like region (white shaded region in Fig. 1*D*) into "catch" regions and "slip" regions, and the switch occurs when the saddle point crosses the switch line from one region into the other.

A switch line extends from its switch point in the direction perpendicular to the force coupling $\boldsymbol{\ell}$, before beginning to bend. More precisely, within a third-order Taylor expansion of $V(\boldsymbol{x})$ around a switch point, the switch line is a straight line perpendicular to $\boldsymbol{\ell}$, and it bends as fourth-order (and higher) terms in $V(\boldsymbol{x})$ become important (33). The exact path of a switch line can be numerically determined using a procedure defined in *SI Appendix*, section 6.

We note that the point at which $E_b(f)$ switches from increasing to decreasing is slightly different than the point where $\tau(f)$ switches from increasing to decreasing. This is because the prefactor τ_0 in Eq. **2** has a mild force dependence (which we account for by solving the Fokker–Planck equation). *SI Appendix*, Fig. S2 shows this difference for the selectin–ligand bonds shown in Figs. 2 and 3.

Data, Materials, and Software Availability. Python code has been deposited at https://github.com/cbarkan1/Selectin_catch_bonding.git (57). Previously published data were used for this work (6, 15, 46, 47).

ACKNOWLEDGMENTS. C.O.B. thanks David Bensimon and Wendy Thomas for illuminating discussions. C.O.B. is grateful for support from the NSF Graduate Research Fellowship (NSF Grant No. DGE-2034835) and the Systems and Integrative Biology Training Grant (NIH Grant No. T32GM008185).

1. C. Zhu, Y. Chen, L. A. Ju, Dynamic bonds and their roles in mechanosensing. *Curr. Opin. Chem. Biol.* **53**, 88–97 (2019).
2. G. Stirnemann, Recent advances and emerging challenges in the molecular modeling of mechanobiological processes. *J. Phys. Chem. B* **126**, 1365–1374 (2022).
3. R. P. McEver, C. Zhu, Rolling cell adhesion. *Annu. Rev. Cell Dev. Biol.* **26**, 363 (2010).
4. J. Z. Kechagia, J. Ivaska, P. Roca-Cusachs, Integrins as biomechanical sensors of the microenvironment. *Nat. Rev. Mol. Cell Biol.* **20**, 457–473 (2019).
5. A. V. Belyaev, I. V. Fedotova, Molecular mechanisms of catch bonds and their implications for platelet hemostasis. *Biophys. Rev.* **15**, 1–24 (2023).
6. B. T. Marshall *et al.*, Direct observation of catch bonds involving cell-adhesion molecules. *Nature* **423**, 190–193 (2003).
7. W. Thomas *et al.*, Catch-bond model derived from allostery explains force-activated bacterial adhesion. *Biophys. J.* **90**, 753–764 (2006).
8. F. Kong, A. J. García, A. P. Mould, M. J. Humphries, C. Zhu, Demonstration of catch bonds between an integrin and its ligand. *J. Cell Biol.* **185**, 1275–1284 (2009).
9. B. Liu, W. Chen, B. D. Evavold, C. Zhu, Accumulation of dynamic catch bonds between TCR and agonist peptide-MHC triggers T cell signaling. *Cell* **157**, 357–368 (2014).
10. C. D. Buckley *et al.*, The minimal cadherin-catenin complex binds to actin filaments under force. *Science* **346**, 1254211 (2014).
11. B. Guo, W. H. Guilford, Mechanics of actomyosin bonds in different nucleotide states are tuned to muscle contraction. *Proc. Natl. Acad. Sci. U.S.A.* **103**, 9844–9849 (2006).
12. R. Litvinov, J. Weisel, Shear strengthens fibrin: The knob-hole interactions display "catch-slip" kinetics. *J. Thromb. Haemost.* **11**, 1933–1935 (2013).
13. S. Rakshit, Y. Zhang, K. Manibog, O. Shafraz, S. Sivasankar, Ideal, catch, and slip bonds in cadherin adhesion. *Proc. Natl. Acad. Sci. U.S.A.* **109**, 18815–18820 (2012).
14. B. Akiyoshi *et al.*, Tension directly stabilizes reconstituted kinetochore-microtubule attachments. *Nature* **468**, 576–579 (2010).
15. A. M. Wayman, W. Chen, R. P. McEver, C. Zhu, Triphasic force dependence of e-selectin/ligand dissociation governs cell rolling under flow. *Biophys. J.* **99**, 1166–1174 (2010).
16. D. Bartolo, I. Derényi, A. Ajdari, Dynamic response of adhesion complexes: Beyond the single-path picture. *Phys. Rev. E* **65**, 051910 (2002).
17. E. Evans, A. Leung, V. Heinrich, C. Zhu, Mechanical switching and coupling between two dissociation pathways in a P-selectin adhesion bond. *Proc. Natl. Acad. Sci. U.S.A.* **101**, 11281–11286 (2004).
18. Y. V. Pereverzev, O. V. Prezhdo, M. Forero, E. V. Sokurenko, W. E. Thomas, The two-pathway model for the catch-slip transition in biological adhesion. *Biophys. J.* **89**, 1446–1454 (2005).
19. V. Barsegov, D. Thirumalai, Dynamics of unbinding of cell adhesion molecules: Transition from catch to slip bonds. *Proc. Natl. Acad. Sci. U.S.A.* **102**, 1835–1839 (2005).
20. J. Lou, C. Zhu, A structure-based sliding-rebinding mechanism for catch bonds. *Biophys. J.* **92**, 1471–1485 (2007).
21. Y. Suzuki, O. K. Dudko, Single-molecule rupture dynamics on multidimensional landscapes. *Phys. Rev. Lett.* **104**, 048101 (2010).
22. S. S. M. Konda, S. M. Avdoshenko, D. E. Makarov, Exploring the topography of the stress-modified energy landscapes of mechanosensitive molecules. *J. Chem. Phys.* **140**, 104114 (2014).
23. S. Chakrabarti, M. Hinczewski, D. Thirumalai, Plasticity of hydrogen bond networks regulates mechanochemistry of cell adhesion complexes. *Proc. Natl. Acad. Sci. U.S.A.* **111**, 9048–9053 (2014).
24. S. Adhikari, J. Moran, C. Weddle, M. Hinczewski, Unraveling the mechanism of the cadherin-catenin-actin catch bond. *PLoS Comput. Biol.* **14**, e1006399 (2018).
25. R. P. McEver, Selectins: Initiators of leucocyte adhesion and signalling at the vascular wall. *Cardiovas. Res.* **107**, 331–339 (2015).
26. Y. Suzuki, O. K. Dudko, Biomolecules under mechanical stress: A simple mechanism of complex behavior. *J. Chem. Phys.* **134**, 065102 (2011).
27. S. S. M. Konda *et al.*, Molecular catch bonds and the anti-Hammond effect in polymer mechanochemistry. *J. Am. Chem. Soc.* **135**, 12722–12729 (2013).
28. S. M. Avdoshenko, D. E. Makarov, Reaction coordinates and pathways of mechanochemical transformations. *J. Phys. Chem. B* **120**, 1537–1545 (2016).
29. D. E. Makarov, Perspective: Mechanochemistry of biological and synthetic molecules. *J. Chem. Phys.* **144**, 030901 (2016).
30. W. Quapp, J. M. Bofill, Reaction rates in a theory of mechanochemical pathways. *J. Comput. Chem.* **37**, 2467–2478 (2016).
31. W. Quapp, J. M. Bofill, J. Ribas-Ariño, Analysis of the acting forces in a theory of catalysis and mechanochemistry. *J. Phys. Chem. A* **121**, 2820–2838 (2017).
32. W. Quapp, J. M. Bofill, J. Ribas-Ariño, Toward a theory of mechanochemistry: Simple models from the very beginnings. *Int. J. Quant. Chem.* **118**, e25775 (2018).
33. C. O. Barkan, R. F. Bruinsma, Catch-slip bonding, pathway switching, and singularities in the flow of molecular deformation. *Phys. Rev. Res.* **5**, 023161 (2023).
34. T. A. Springer, Structural basis for selectin mechanochemistry. *Proc. Natl. Acad. Sci. U.S.A.* **106**, 91–96 (2009).
35. N. S. Astrof, A. Salas, M. Shimaoka, J. Chen, T. A. Springer, Importance of force linkage in mechanochemistry of adhesion receptors. *Biochemistry* **45**, 15020–15028 (2006).
36. G. I. Bell, Models for the specific adhesion of cells to cells: A theoretical framework for adhesion mediated by reversible bonds between cell surface molecules. *Science* **200**, 618–627 (1978).
37. V. Barsegov, D. Thirumalai, Dynamic competition between catch and slip bonds in selectins bound to ligands. *J. Phys. Chem. B* **110**, 26403–26412 (2006).
38. L. M. Nilsson, W. E. Thomas, E. V. Sokurenko, V. Vogel, Beyond induced-fit receptor-ligand interactions: Structural changes that can significantly extend bond lifetimes. *Structure* **16**, 1047–1058 (2008).
39. P. Wu *et al.*, Mechano-regulation of peptide-MHC class i conformations determines TCR antigen recognition. *Mole. Cell* **73**, 1015–1027 (2019).
40. H. K. Choi *et al.*, Catch bond models may explain how force amplifies TCR signaling and antigen discrimination. *Nat. Commun.* **14**, 2616 (2023).
41. K. D. Patel, M. U. Nollert, R. P. McEver, P-selectin must extend a sufficient length from the plasma membrane to mediate rolling of neutrophils. *J. Cell Biol.* **131**, 1893–1902 (1995).
42. W. S. Somers, J. Tang, G. D. Shaw, R. T. Camphausen, Insights into the molecular basis of leukocyte tethering and rolling revealed by structures of P-and E-selectin bound to SLeX and PSGL-1. *Cell* **103**, 467–479 (2000).
43. T. T. Waldron, T. A. Springer, Transmission of allostery through the lectin domain in selectin-mediated cell adhesion. *Proc. Natl. Acad. Sci. U.S.A.* **106**, 85–90 (2009).
44. J. S. Langer, Statistical theory of the decay of metastable states. *Ann. Phys.* **54**, 258–275 (1969).
45. K. K. Sarangapani *et al.*, Low force decelerates l-selectin dissociation from P-selectin glycoprotein ligand-1 and endoglycan. *J. Biol. Chem.* **279**, 2291–2298 (2004).
46. J. Lou *et al.*, Flow-enhanced adhesion regulated by a selectin interdomain hinge. *J. Cell Biol.* **174**, 1107–1117 (2006).
47. A. G. Klopocki *et al.*, Replacing a lectin domain residue in l-selectin enhances binding to P-selectin glycoprotein ligand-1 but not to 6-sulfo-sialyl Lewis x. *J. Biol. Chem.* **283**, 11493–11500 (2008).
48. W. Cai *et al.*, Anisotropic friction in a ligand-protein complex. *Nano Lett.* **23**, 4111–4119 (2023).
49. D. K. Das *et al.*, Force-dependent transition in the T-cell receptor β-subunit allosterically regulates peptide discrimination and pMHC bond lifetime. *Proc. Natl. Acad. Sci. U.S.A.* **112**, 1517–1522 (2015).
50. M. M. Sauer *et al.*, Catch-bond mechanism of the bacterial adhesin FimH. *Nat. Commun.* **7**, 10738 (2016).
51. G. R. Heath *et al.*, Localization atomic force microscopy. *Nature* **594**, 385–390 (2021).
52. G. Volpe *et al.*, Roadmap for optical tweezers. *J. Phys.: Photon.* **5**, 022501 (2023).
53. B. Hellenkamp *et al.*, Precision and accuracy of single-molecule fret measurements-a multi-laboratory benchmark study. *Nat. Methods* **15**, 669–676 (2018).
54. W. J. Peña Ccoa, G. M. Hocky, Assessing models of force-dependent unbinding rates via infrequent metadynamics. *J. Chem. Phys.* **156**, 125105 (2022).
55. G. G. Stokes, On the effect of the internal friction of fluids on the motion of pendulums. *Trans. Cambr. Philos. Soc.* **9**, 8–106 (1851).
56. F. H. Branin, Widely convergent method for finding multiple solutions of simultaneous nonlinear equations. *IBM J. Res. Dev.* **16**, 504–522 (1972).
57. C. O. Barkan, Python code to reproduce figures. cbarkan1/Selectin_catch_bonding. Github. https://github.com/cbarkan1/Selectin_catch_bonding.git. Deposited 18 January 2024.